SSRG International Journal of Electrical and Electronics Engineering
ISSN: 2348-8379/ https://doi.org/10.14445/23488379/IJEEE-V13I8P101

Volume 13 Issue 8, 1-10, August 2026
© 2026 Seventh Sense Research Group®

Original Article

Novel Surface Electromyography-based Movement Intent Identification Method using Kalman Filtering and K-Nearest Neighbors to Control an Exoskeleton Robot

Tri Nguyen[1], Dinh-Hung Tran[2,3], Thi-Duyen Bui[2], Tran-Thang Le[1], Ngoc-Khoat Nguyen[2*]

[1]*Control Automation in Production and Improvement of Technology Institute (CAPITI), Academy of Military Science and Technology, Hanoi, Vietnam.*
[2]*Faculty of Control and Automation, Electric Power University, Hanoi, Vietnam.*
[3]*Viettel Aerospace Institute - Viettel Military Industry and Telecoms Group, Hanoi, Vietnam.*

**Corresponding Author : khoatnn@epu.edu.vn*

Received: 14 May 2026 Revised: 23 June 2026 Accepted: 22 July 2026 Published: 25 August 2026

Abstract - *The purpose of this paper is to identify a novel hybrid control architecture for exoskeleton robot movement using Surface Electromyography (sEMG) signals. It addresses instability and 'label flickering' in machine learning by using a parallel set of 54 independent Kalman-filtered features applied directly in the feature space. Based on 9-channel data from the SIAT-LLMD dataset, this work extracts 6 time-domain features using 200 ms sliding windows, including: RMS, MAV, WL, SSI, DASDV and ZC. After extracting meaningful features, the signals are smoothed using an efficient 1D Kalman filter. The result is a 64.7% reduction of noise for training the K-Nearest Neighbors (KNN) model with the factor k equals 1. From significant simulation results, the proposed engineering method meets the real-time requirements of a lower extremity exoskeleton robotic control system by achieving 99.1% classification accuracy on a 16-class test dataset with execution times under 100ms per window. To assess the control relevance of the decoded intent, an sEMG-modulated Fuzzy-PI controller was compared with PID and boundary-layer Sliding-Mode Control (SMC) on a three-degree-of-freedom lower-limb exoskeleton under parameter uncertainty, actuator constraints, and load disturbances. Fuzzy-PI attained a mean tracking RMSE of 2.977°, corresponding to reductions of 48.6% and 46.1% relative to PID and SMC, respectively, without a material increase in RMS actuator torque. The combined recognition-and-control framework, therefore, provides a computationally efficient route from muscle activity to stable assistive motion. The proposed algorithm offers a good balance for embedded systems in lower extremity rehabilitation robotic applications, but it is also able to be applied for the upper ones, achieving a good balance between accuracy, stability, and computational cost.*

Keywords - *Kalman filter, K-Nearest Neighbors, Exoskeleton robot, Movement Intent Recognition, Surface Electromyography.*

1. Introduction

These days, healthcare systems are under pressure due to an aging population and the increase in incidence of neuromotor disorders such as stroke and spinal cord injuries. To solve this problem, exoskeletons and robotic rehabilitation devices have emerged, enabling the implementation of high-intensity training programs. However, the key to accelerating neurological recovery is the level of active patient interaction. For this reason, robots need to be upgraded to Human-Machine Interface (HMI) capabilities to interpret the patient's movement intentions from surface Electromyography (sEMG) signals and respond quickly to those intended movements.

The sEMG method records the electrical activity which is created by skeletal muscles through electrodes placed on the skin. Then, it can provide an anticipatory signal for intention-driven human-machine interfaces. A recent review identifies electrode-placement sensitivity, inter- and intra-subject physiological variability, motion-induced artifacts, and the inherent non-stationarity of sEMG signals as principal challenges to achieving robust intention and movement recognition [1]. Deep-learning approaches can improve representation learning, although their data and computational requirements complicate low-power embedded implementation [2].

A demographically diverse sEMG database further highlights the need to account for inter-subject distribution shifts when assessing model generalizability [3]. In exoskeleton applications, sensing and control architectures must also meet stringent requirements for safety, user comfort, and real-time human-robot interaction [4].

This is an open access article under the CC BY-NC-ND license (http://creativecommons.org/licenses/by-nc-nd/4.0/)

It has been known that a lot of studies have been conducted on the processing of sEMG signals based on deep learning techniques. With the extremely fast development of artificial intelligence, deep learning has been applied to this kind of signal processing to enhance the classification accuracy. However, the contrast is that the computation needs should often be high, affecting the real-time response of the exoskeleton robot. In this aspect, this word proposes a novel hybrid model with light weight of computation. Such a processing architecture has a good feature of identifying the real-time human walking intent without overloading it to be overloaded. Theoretically, the mechanism proposed in this work concludes several phases as mentioned below:

- Compact time-domain feature extraction.
- The application of one-dimensional Kalman filtering directly on the feature space to smooth trajectories and eliminate flickering.
- A Fine K-Nearest Neighbors (KNN, with $k = 1$) classifier.

It is confirmed that while maintaining strict real-time performance with minimal hardware requirements, the resulting system can obtain exceptional accuracy. As a result, the model which is studied in this work can completely be able to be integrated into the control system for exoskeleton robots. The next section will present related work with existed reports motivating the current study.

2. Related Work

2.1. Traditional Machine Learning and the Feature Noise Problem

Recent open-access databases have strengthened reproducibility and enabled more consistent benchmarking of lower-limb movement-intent recognition methods. The SIAT-LLMD dataset contains synchronized nine-channel sEMG, kinematic, and kinetic recordings from 40 participants performing 16 classes of lower-limb movement [5]. Moreira et al. reported lower-limb kinematic, kinetic, and EMG data during controlled-speed walking [6]. Reznick et al. published a dataset from 10 volunteers characterizing continuously varying locomotion, including transitions between distinct locomotor tasks and conditions [7]. Camargo et al. introduced an open-source lower-limb biomechanics dataset which collected from 22 participants, including stair ascent and descent, ramp negotiation, level-ground walking, and transitions between these locomotion modes [8]. The HAR-sEMG database supplies labeled lower-limb sEMG activities for evaluating compact recognition algorithms [9].

2.2. Recent Recognition, Estimation, and Embedded-Deployment Studies

More recent datasets have expanded the range of sensing modalities and experimental conditions available for algorithm development. Dimitrov et al. reported synchronized high-density sEMG, IMU, kinetic, and kinematic measurements acquired during multiple locomotor activities collected from 10 volunteers [10]. Schulte et al. introduced a multi-session database comprising lower-limb kinematics and sEMG recordings collected under different electrode configurations during gait-related activities [11]. The Gait120 dataset further extended multimodal locomotion analysis to 120 participants performing seven common daily movement tasks [12]. For feature-based recognition, Wang et al. introduced a weighted-feature method for classifying lower-limb actions from sEMG [13]. A separate study by Wang et al. analyzed and recognized lower-limb motions using conventional EMG signal descriptors and machine-learning classifiers [14].

Zhou et al. integrated wearable sEMG and accelerometer signals to recognize ankle-foot movements for the control of a smart ankle-foot orthosis [15]. Wang et al. developed a multi-branch neural network to estimate lower-limb movement continuously from multichannel sEMG signals [16].

Recursive estimation methods have also been examined in myoelectric interfaces. Dutra et al. combined a state-space model with Kalman filtering to estimate grasping force continuously from sEMG, illustrating the benefit of recursive state estimation for attenuating measurement variability [17]. Rabe et al. compared sonomyographic and electromyographic sensing for continuous joint-torque estimation during ambulation across multiple terrains [18].

For gait-event decoding, Morbidoni et al. applied machine-learning techniques to predict gait events from EMG recordings in children with cerebral palsy [19]. Liu et al. introduced a deep-learning fusion architecture for recognizing dynamic muscle-fatigue states, underscoring the need to account for fatigue-related temporal changes in practical sEMG systems [20]. Haufe et al. evaluated the feasibility of predicting gait events from sEMG signals in individuals with Parkinson's disease [21]. Tigrini et al. developed a computationally efficient feature-extraction method based on phasor representations of myoelectric synergies to enhance gait-phase recognition [22].

Mengarelli et al. estimated vertical ground-reaction force during unconstrained walking with a stacked one-dimensional convolutional long short-term memory model [23]. Ye et al. implemented online lower-limb movement recognition from sEMG and demonstrated its use in real-time rehabilitation training [24]. Liu et al. estimated multiple gait parameters from lower-limb sEMG using Random Forest, CatBoost, and XGBoost models, while also showing that muscle-fatigue condition affects model performance [25]. Collectively, these studies demonstrate improving accuracy and task coverage, but they also expose persistent deployment issues involving short-window variability, subject dependence, transition ambiguity, memory demand, and inference latency.

2.3. Research Gap and Motivation

The literature indicates a recurring trade-off between computational efficiency and representational capacity. Compact, feature-based methods are generally suitable for real-time implementation but remain susceptible to measurement noise, muscle fatigue, inter-subject variability, and transitions between locomotor conditions. Conversely, multimodal and deep-learning approaches can capture more complex signal patterns, although their computational and implementation requirements are typically higher. Existing studies commonly suppress noise at the raw-signal stage or incorporate temporal dependencies within relatively complex estimators. By comparison, the independent temporal smoothing of individual feature trajectories before classification has received limited attention.

This observation motivates the proposed framework, in which 54 one-dimensional Kalman filters are applied separately to the extracted feature sequences before classification using Fine KNN. The design aims to reduce short-term variability in the feature space while retaining a computationally lightweight classification architecture.

3. Methodology

The proposed control methodology for an exoskeleton robot using sEMG is drawn in Figure 1. As shown, the system typically includes several main phases below:

Phase (1): sEMG data acquisition. The raw signals of sEMG are acquired from the muscles of the user in this phase.

Phases (2)-(4): signal processing. The sEMG signals, after being preprocessed to remove noise and/or undesired signal distortions, are processed by using a proper method, i.e. sliding window segmentation. Then, a number of meaningful features in time or frequency domains are extracted.

Phases (5)-(7): Filtering, normalizing and generating command. The extracted features with highly meaningful values are smoothed using an effective filter, such as a Kalman one, to enhance the stability and reliability. A normalization and movement intention classification are necessary before creating a high-level control command at the end of these phases.

Phases (8)-(9): Control of the exoskeleton robot. With the significant control signal taken from the previous phase, it will be employed for controlling the exoskeleton robot. It is noted that in these phases, an efficient control strategy will also be applied. A number of controllers are successfully used for the exoskeleton robot: PID, impedance and intelligent controllers. Remember that the intelligent regulators used successfully for the exoskeleton robots include fuzzy logic, artificial neural network and metaheuristic optimizations- based ones.

Phases (10)-(11): Robot to assist disabilities with closed-loop control. It is significant that, together with the assistance to disabled users, the safety monitoring and sensor feedback part may form a closed-loop control architecture. This structure is typically built to continuously update the output signal in a highly efficient control system, especially in a real-time robot like an assisted exoskeleton.

As a first step of a full project, this study focuses primarily on the problem of processing sEMG signals. The control of human limbs, including lower and upper ones, is similar, especially in the sEMG signal processing. The current work selected the lower limb as a case study, meaning that, for the upper limbs, the signal processing is completely analogous. With the sEMG signal of lower limbs, three pipelines on the same SIAT-LLMD dataset (40 subjects, 16 classes, 9 channels, 200 ms windows, 50% overlap) are chosen in the current work.

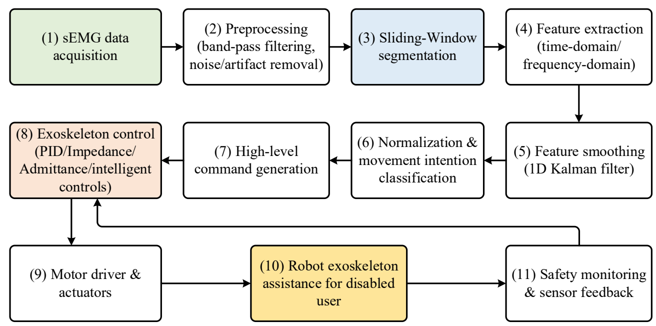

Fig. 1 sEMG Signal processing and sEMG-based control system for exoskeleton robots: a block diagram

3.1. sEMG Signal Data

This study uses the publicly available SIAT-LLMD dataset for experimental evaluation [5]. The dataset comprises synchronized sEMG, kinematic, and kinetic recordings from 40 healthy participants, with reported mean values of 24.5 years for age, 63.8 kg for body mass, and 1.693 m for height. Each participant performed 16 lower-limb movement classes encompassing static postures, level walking, stair ascent and descent, sit-to-stand transitions, lunges, knee lifts, and gait-related foot-contact conditions. Nine sEMG channels were recorded from muscles of the left lower limb, while motion-capture and force-plate measurements supported movement labeling and biomechanical characterization. Full details of the acquisition protocol, sensor placement, and movement definitions are available in the original dataset publication.

In the present work, these data are used to evaluate the proposed signal-processing and classification pipeline for prospective exoskeleton-control applications. During preprocessing, a 20-450 Hz band-pass filter is applied to attenuate low-frequency motion artifacts and high-frequency interference while preserving the principal frequency content of the sEMG signals.

3.2. Sliding-Window Segmentation and Feature Extraction

The robot control problem involves a continuous data stream. To balance statistical information and command latency, a sliding window of L = 200 ms (N = 200 samples after resampling) is used with 50% overlap, corresponding to a 100 ms stride. Thus, an updated prediction is generated every 100 ms. Six low-cost time-domain descriptors, including RMS, MAV, WL, SSI, DASDV, and ZC, are extracted from each window because compact sEMG descriptors remain effective for lower-limb action recognition [13]. Table 1 summarizes the six features used in the proposed pipeline.

Table 1. Six meaningful time-domain features of sEMG signals

Features	Formula
Root Mean Square (RMS)	$\text{RMS} = \sqrt{\frac{1}{N}\sum_{i=1}^{N} x_i^2}$ (1)
Mean Absolute Value (MAV)	$\text{MAV} = \frac{1}{N}\sum_{i=1}^{N} \mid x_i \mid$ (2)
Waveform Length (WL)	$\text{WL} = \sum_{i=1}^{N-1} \mid x_{i+1} - x_i \mid$ (3)
Simple Square Integral (SSI)	$\text{SSI} = \sum_{i=1}^{N} x_i^2$ (4)
Difference Absolute Standard Deviation Value (DASDV)	$DASDV = \sqrt{\frac{1}{N-1}\sum_{i=1}^{N-1}(x_{i+1} - x_i)^2}$ (5)
Zero Crossing (ZC)	$\text{ZC} = \sum_{i=1}^{N-1}[I(x_i \cdot x_{i+1} < 0)$ and $\mid x_i - x_{i+1} \mid \geq \epsilon]$ (6)

It is noted that the signal processing execution should deal with a feature matrix in a 54-dimensional space resulting from nine channels of the sEMG sensors. The computation of this combination has a complexity of only O(N), completely relieving the burden on the embedded processor.

3.3. Applying One-D Kalman Filter to Trajectories of the Features

Motivated by recursive state-space smoothing in myoelectric estimation [17], this work constructs 54 independent One-Dimensional (1D) Kalman filters that operate in parallel on the extracted feature trajectories. Each filter tracks one feature across successive windows. Because physiological movement intention changes continuously rather than arbitrarily between adjacent windows, a feature value s at time step k is modeled using the following linear Markov state and measurement equations.

$$s_k = s_{k-1} + w_{k-1} \tag{7}$$

$$z_k = s_k + v_k \tag{8}$$

In (7), the factor s_k can be considered a right feature value to be estimated. Meanwhile, the other factor z_k is the raw feature value computed from the *k-th* window, $w_{k-1} \sim \mathcal{N}(0, Q)$ is the process noise covariance; and $v_k \sim \mathcal{N}(0, R)$ is the measurement noise covariance (sEMG physiological noise). The following cycle is designed to perform the optimal recursive filtering process for each value.

Stage 1: Predict period. In this phase, the state at step k, which is based on information taken from step k-1, should be forecasted. The state prediction should be:

$$\hat{s}_{k|k-1} = \hat{s}_{k-1|k-1} \tag{9}$$

In this phase, the error covariance prediction is calculated as follows:

$$P_{k|k-1} = P_{k-1|k-1} + Q \tag{10}$$

Stage 2: Update phase. In this phase, it is necessary to fix the predict process by employing the real measurements. Three sub-periods are applied below:

(i) Compute the Kalman gain as

$$K_k = \frac{P_{k|k-1}}{P_{k|k-1} + R} \tag{11}$$

(ii) An approximate update for the empirical process should be employed

$$\hat{s}_{k|k} = \hat{s}_{k|k-1} + K_k(z_k - \hat{s}_{k|k-1}) \tag{12}$$

(iii) An updating process for the error covariance is executed

$$P_{k|k} = (1 - K_k)P_{k|k-1} \tag{13}$$

In the cycle above, the power of the Kalman filter relies on a reasonable ratio, and it should be configured with a very small value of Q. This parameter reflects the steady nature of motion intent. Besides, the filter creates a high value for R, which is a factor accounting for the inherent uncertainty in the sEMG output computing results. It should be confirmed that an excellent smoothness with 64.7% removal of random variance is obtained during such a filtering process. It is explained due to the change in intensity in response to the noise. In addition, the point data in 54-dimensional space can be seen as it is converged into defined domains, which show 16 motion categories. Before entering classification, the feature vector is normalized to global standard deviation normalization (Z-score normalization) to a scale suitable for basic surveys.

3.4. Fine KNN-based Non-Linearity Exploitation

It is found that the KNN executed in the machine learning space has a drawback of lacking an explicit training phase. In this perspective, the model uses a Euclidean distance function given in (14) to classify a test data sample $x \in \mathbb{R}^{54}$.

$$d(x, y) = \sqrt{\sum_{j=1}^{54}(x_j - y_j)^2} \tag{14}$$

This work uses a Fine KNN model with k = 1 as the classifier for the 16-class problem after Kalman smoothing. Recent lower-limb sEMG research confirms that compact feature-based classification remains attractive for real-time recognition [13]. Although k = 1 is normally vulnerable to noise and overfitting, the proposed Kalman stage regularizes the 54-dimensional feature space before classification. The cleaned local neighborhoods then allow Fine KNN to capture nonlinear decision boundaries with a small computational footprint suitable for real-time embedded execution.

4. Proposed System Behavior Prediction Architecture

4.1. Real-Time System Architecture Overview

The signal processing architecture presented in Section 3 not only instantaneously identifies lower limb movement intentions but also predicts long-term system behavior patterns (e.g., subsequent gait phase and adaptive torque support), serving as a solid foundation for next-generation lower limb rehabilitation robots and exoskeletons.

This architecture operates by processing data continuously, optimizing resources to run entirely on embedded microcontrollers, and the process is divided into five main phases:

(1) sEMG Signal Acquisition and Preprocessing: Collects 9 channels of sEMG at a 1000 Hz sampling rate (interpolated from 1926 Hz). Applies a 2nd-order IIR Notch Filter ($f_c = 50$ Hz) followed by a 4th-order Butterworth Bandpass filter ($f_{low} = 20$ Hz, $f_{high} = 450$ Hz).
(2) Segmentation and Compact Feature Extraction: Utilizes a sliding window of 200 ms with a 50% overlap (100 ms stride). Extracts 6 time-domain features, generating a raw feature vector $z_k \in \mathbb{R}^{54}$.
(3) Trajectory Smoothing via 54 Parallel 1D Kalman Filters: Each feature dimension is processed independently by a Kalman filter configured with $Q = 1 \times 10^{-6}$ and $R = 5 \times 10^{-2}$. Output: a smoothed feature vector $\hat{f}_{54}$.
(4) Normalization and Classification: Global Z-score normalization → Fine KNN $k = 1$, Euclidean distance) → outputs a movement label (1 of 16 classes) every 100 ms.
(5) System Behavior Prediction Layer: Leverages the label sequence and feature vectors from the 5-10 most recent frames to predict the subsequent gait cycle phase and the desired level of assistive torque (0-100% torque assistance).

4.2. Scientific and Technical Rationale

The proposed method mentioned above is based on the following factors of the rationale:

- Noise suppression: The parallel Kalman filters reduce random noise variance by 64.7%, effectively minimizing label flickering during movement transitions.
- Low latency: The complete pipeline operates with linear computational complexity. It achieves an inference time of under 10 ms on a Cortex-M7 microcontroller, comfortably satisfying the strict < 100 ms requirement for real-time exoskeleton control.
- Nonlinear classification: Following the feature smoothing stage, the Fine KNN (k = 1) model accurately delineates complex decision boundaries.
- Embedded feasibility: Operating as a lazy learner, the model eliminates the need for explicit retraining and requires a memory footprint of approximately 50-80 MB, making it viable for embedded deployment.
- Scalability: The architecture can seamlessly integrate additional sensor modalities (e.g., IMUs, force plates, joint encoders) without altering the core algorithmic structure.

Following the above analysis, Figure 2 shows the system framework for action pattern prediction to control the exoskeleton robots.

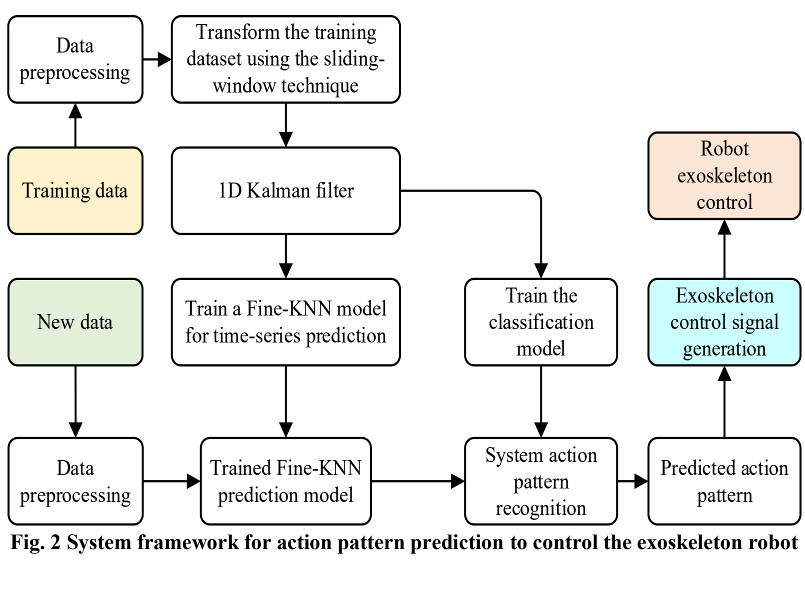

Fig. 2 System framework for action pattern prediction to control the exoskeleton robot

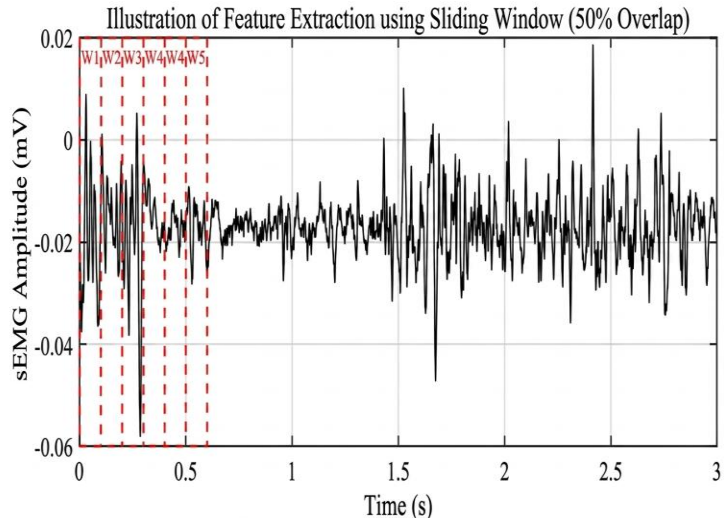

Fig. 3 sEMG Signal segmentation process using a sliding window technique with 50% overlap

5. Experimental Results and Evaluation

5.1. Experimental Setup

All experiments were carried out using the SIAT-LLMD dataset in order to thoroughly assess the efficacy of the suggested strategy. This SIAT-LLMD dataset has 40 subjects and 16 lower limb movement classes. The collected samples from 9 channels were recorded as raw sEMG signals, and they were interpolated to 1000 Hz, following the designed steps.

Data segmentation was done using a 200 ms sliding window with a 50% overlap, which is equivalent to a 100 ms stride. Exactly 54 time-domain features were taken from 9 channels (6 features × 9 channels).

For the 1D Kalman filter, the process noise $Q = 10^{-6}$ and the measurement noise was $R = 5 \times 10^{-2}$. Once the Z-score normalization was done, we used the hold-out method to split the set into 80% training and 20% testing.

The system ran a Fine KNN model with k = 1 and Euclidean distance for classification. Finally, Neighborhood Component Analysis (NCA) are applied to pick the most important features and fix the feature space.

5.2. Evaluation of Feature Extraction and Optimization

5.2.1. Impact of the Sliding Window Technique

The use of a 200 ms window length ensures the full extraction of statistical information from the signals. The system meets real-time requirements because the latency is under 100 ms.

Applying a 50% overlap between windows help increasing the density of the training samples and prevents information loss at the window boundaries. This process generates a continuous and smooth feature sequence, which is highly suitable for streaming data recognition.

5.2.2. Efficacy of the Kalman Filter on the Feature Space

An analytical juxtaposition embodied in Figure 4 delineates the RMS-based trajectory bifurcations, contrasting the pre-processing phase against the subsequent Kalman-filtered execution.

As can be seen, the raw features exhibit significantly high-frequency fluctuations and lack temporal stability. Paradoxically, the filtration's byproduct is a crystalline fluidic motion that mutes stochastic interference yet anchors the primordial kinematic signature. Clusters crystallize within the manifold, a direct consequence of variance-sensitive KNN logic reacting to the purged noise.

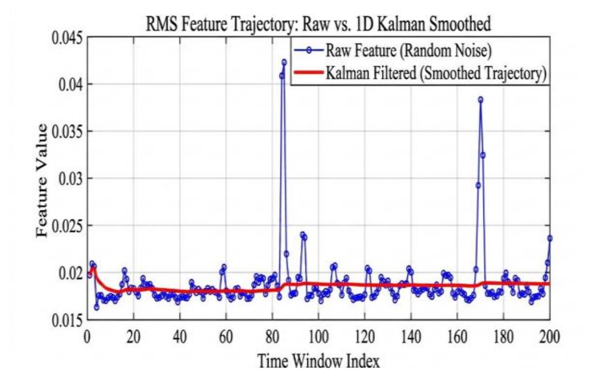

Fig. 4 Comparison of the RMS feature before and after applying the Kalman filter

5.2.3. Feature Importance Analysis (NCA) and Model Optimization

Checking the NCA outcomes in Figure 5, it is obvious that those 54 features do not contribute equally to the final classification performance. Particularly, information redundancy is indicated by the weights of several feature dimensions being close to zero. However, strong discriminative power is provided by some features that retain high weights > 0.5.

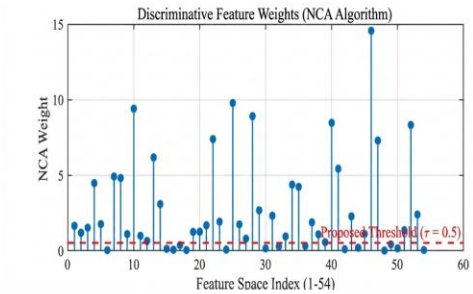

Fig. 5 Weights of the 54 features calculated by the NCA algorithm

5.2.4. Model Optimization: Accuracy versus Model Size

The trade-off between accuracy and model size is shown in Figure 6. It shows that incremental feature removal significantly reduces model size while only slightly reducing a slight accuracy. An optimal point appears at the NCA threshold of approximately 0.5. At this specific point, removing the feature set reduces the complexity of the basic operations and increases inference speed. Nevertheless, the system somehow preserves a formidable degree of precision.

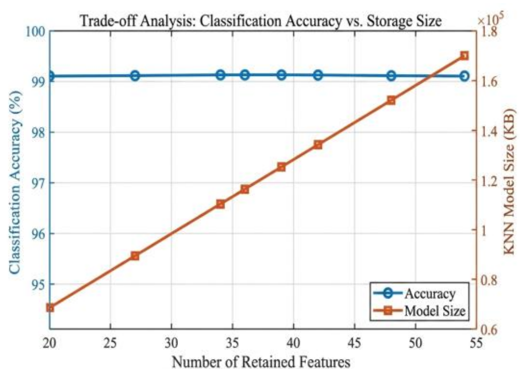

Fig. 6 Evaluation of the trade-off between accuracy and storage cost across different feature selection thresholds

5.2.5. Evaluation of Classification Model Performance

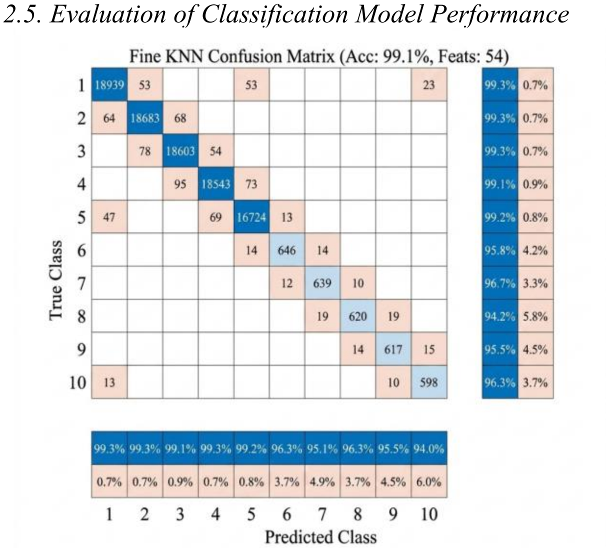

Fig. 7 An illustration of the confusion matrix resulting from the classification model corresponding to 16 movements of the human

5.3. Comparison with State-of-the-Art Methods

The Fine KNN classifier (k = 1, Euclidean distance) in conjunction with the Kalman filter produced the highest classification accuracy of 99.1% of all assessed models, as Table 2 illustrates. It continuously performed better than the Fine Gaussian SVM and other KNN variations. Importantly, an ablation study was carried out to show the crucial significance of our suggested architecture. The classification accuracy dropped rapidly to 85.1% when the Fine KNN classifiers were applied directly to the raw extracted features without Kalman filtering.

This direct comparison shows that the greater 99.1% accuracy is not merely a byproduct of the KNN algorithm but is mostly caused by the Kalman filter's capacity to purify the feature space and remove label flickering.

These result highlights the perfect synergy between Kalman smoothing and the local, nonlinear decision boundaries of Fine KNN. Furthermore, this also creates a highly efficient, state-of-the-art model that is suitable for real-time embedded deployment in rehabilitation exoskeleton systems.

Table 2. Performance comparison of different classifiers

Model	Type	Accuracy (%)	Notes
Fine KNN	KNN (k=1, Euclidean)	99.1	Highest, optimal after Kalman smoothing
Weighted KNN	KNN	97.5	Improved stability
Medium KNN	KNN (k=10)	94.2	Balanced over/under-fitting
Cosine KNN	KNN	94.2	Suitable for high-dimensional data
Cubic KNN	KNN	93.9	Smoother decision boundaries using a kernel
Fine Gaussian SVM	SVM	90.2	Gaussian kernel (scale = 0.25)
Fine KNN (Baseline)	KNN (k=1, Euclidean)	85.1	Without Kalman Filter

5.4. Closed-Loop sEMG-Assisted Control Evaluation

The 100 ms intent stream was connected to a sagittal three-joint human-exoskeleton model. Fuzzy-PI, PID, and boundary-layer SMC were evaluated using identical initial conditions, model perturbations of up to approximately 12%, friction, actuator lag, torque and torque-rate limits, and two bounded load disturbances. Kalman-smoothed activation modulated the Fuzzy-PI gains; it was not interpreted as measured biological torque. As shown in Figure 8, the proposed Fuzzy-PI controller follows the reference trajectories closely at all three joints, with particularly improved transient tracking at the knee and ankle. Compared with PID and SMC, Fuzzy-PI produces smaller deviations during rapid trajectory changes and avoids the pronounced overshoot observed in the ankle response. These results indicate that the adaptive gain adjustment of the Fuzzy-PI scheme provides a more consistent balance between tracking accuracy and closed-loop smoothness.

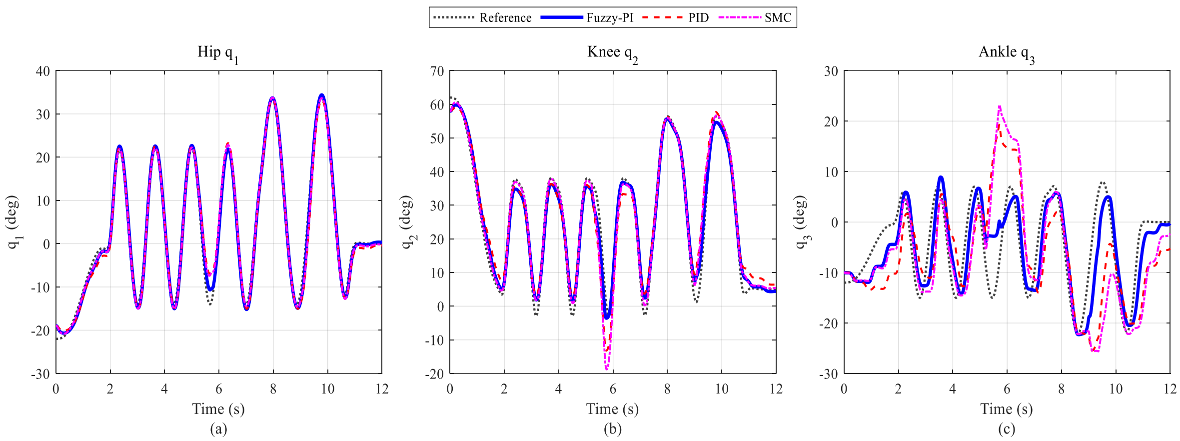

Fig. 8 Three-DOF joint tracking under parameter uncertainty, actuator constraints, and external disturbances

Table 3. Mean closed-loop tracking performance over three joints

Method	RMSE (°)	IAE (°·s)
Fuzzy-PI	2.977	28.523
PID	5.793	53.086
SMC	5.519	42.699

To create a numerical comparison, Table 3 presents the performance concerning the mean closed-loop tracking control over three joints corresponding to the results shown in Figure 8. As summarized in Table 3, the proposed Fuzzy-PI controller achieves the lowest mean RMSE and IAE, reaching 2.977° and 28.523°·s, respectively. Relative to PID and SMC, these values confirm a substantial improvement in overall tracking accuracy and accumulated error across the three joints. Besides, the fuzzy-PI controller reduced mean RMSE by 48.6% relative to PID and by 46.1% relative to SMC. The corresponding mean RMS torques were 7.833, 7.769, and 7.903 N·m, respectively; thus, the tracking improvement did not rely on increased actuator effort. The gain adaptation was most beneficial at gait transitions and disturbance onsets, where fixed PID gains produced larger lag, and SMC retained higher residual error. These deterministic results support Fuzzy-PI as the downstream controller of the Kalman-filtered intent decoder, while hardware and subject-specific validation remain necessary.

6. Conclusion and Future Work

This work successfully proposes and implements a novel architecture, named the Kalman-filtered Fine KNN Real-time Intent Decoder for movement intent recognition using sEMG signals. The proposed method is initially applied to lower limbs, but it is completely able to be used for the upper ones to control an exoskeleton robot. This study contributes in three aspects. First, extracting a compact set of 54 time-domain features. Secondly, pioneering the application of 54 parallel 1D Kalman filters to smooth feature trajectories and effectively reduces random noise variance by 64.7%. Finally, deploying the Fine KNN algorithm k = 1 on the cleaned data space. This demonstrates that the method achieves a high accuracy of 99.1% on the SIAT-LLMD dataset while maintaining a system latency of less than 100 ms. A concise closed-loop evaluation further showed that the decoded command can drive a three-degree-of-freedom lower-limb exoskeleton robot through an sEMG-modulated Fuzzy-PI controller. Under model uncertainty, actuator limits, and external disturbances, the Fuzzy-PI controller lowered the mean RMSE to 2.977° and outperformed PID and SMC without materially increasing RMS torque.

The proposed architecture achieves an optimal balance among high accuracy, strong robustness, and extremely low computational cost. Additionally, compared to conventional deep learning models, it is well-suited for direct deployment on low-power embedded microcontrollers in rehabilitation robots and exoskeleton systems. Therefore, this enables compliance with stringent real-time biosafety requirements. However, a current limitation of this research is that experiments are only conducted on data from healthy subjects. As a result, the future work inspired by the current study will focus on several directions below:

(i) Implementing the algorithm on a dedicated embedded hardware (e.g., STM32H7 series);
(ii) Integrating feedback structures from dynamic sensors (IMUs) and force plates;

(iii) Conducting clinical trials on patients after stroke or spinal cord injury;
(iv) Integrating reinforcement learning mechanisms to optimize the level of motor support appropriate to each patient's physiology.

Acknowledgments

This work presents the research findings of Project No. ĐTKHCN.08/2025, an institutional-level research project at Electric Power University in 2025.

References

[1] Hao Xu, and Anbin Xiong, "Advances and Disturbances in sEMG-based Intentions and Movements Recognition: A Review," *IEEE Sensors Journal*, vol. 21, no. 12, pp. 13019-13028, 2021. [CrossRef] [Google Scholar] [Publisher Link]

[2] Wei Li, Ping Shi, and Hongliu Yu, "Gesture Recognition using Surface Electromyography and Deep Learning for Prostheses Hand: State-of-the-Art, Challenges, and Future," *Frontiers in Neuroscience*, vol. 15, pp. 1-20, 2021. [CrossRef] [Google Scholar] [Publisher Link]

[3] Harshavardhana T. Gowda et al., "A Database of Upper Limb Surface Electromyogram Signals from Demographically Diverse Individuals," *Scientific Data*, vol. 12, no. 1, pp. 1-10, 2025. [CrossRef] [Google Scholar] [Publisher Link]

[4] Athar Ali et al., "Systematic Review of Back-Support Exoskeletons and Soft Robotic Suits," *Frontiers in Bioengineering and Biotechnology*, vol. 9, pp. 1-15, 2021. [CrossRef] [Google Scholar] [Publisher Link]

[5] Wenhao Wei et al., "Surface Electromyogram, Kinematic, and Kinetic Dataset of Lower Limb Walking for Movement Intent Recognition," *Scientific Data*, vol. 10, no. 1, pp. 1-16, 2023. [CrossRef] [Google Scholar] [Publisher Link]

[6] Luís Moreira et al., "Lower Limb Kinematic, Kinetic, and EMG Data from Young Healthy Humans During Walking at Controlled Speeds," *Scientific Data*, vol. 8, no. 1, pp. 1-11, 2021. [CrossRef] [Google Scholar] [Publisher Link]

[7] Emma Reznick et al., "Lower-Limb Kinematics and Kinetics during Continuously Varying Human Locomotion," *Scientific Data*, vol. 8, no. 1, pp. 1-12, 2021. [CrossRef] [Google Scholar] [Publisher Link]

[8] Jonathan Camargo et al., "A Comprehensive, Open-Source Dataset of Lower Limb Biomechanics in Multiple Conditions of Stairs, Ramps, and Level-Ground Ambulation and Transitions," *Journal of Biomechanics*, vol. 119, 2021. [CrossRef] [Google Scholar] [Publisher Link]

[9] Yu Luan et al., "HAR-sEMG: A Dataset for Human Activity Recognition on Lower-Limb sEMG," *Knowledge and Information Systems*, vol. 63, no. 10, pp. 2791-2814, 2021. [CrossRef] [Google Scholar] [Publisher Link]

[10] Hristo Dimitrov, Anthony M.J. Bull, and Dario Farina, "High-Density EMG, IMU, Kinetic, and Kinematic Open-Source Data for Comprehensive Locomotion Activities," *Scientific Data*, vol. 10, no. 1, pp. 1-10, 2023. [CrossRef] [Google Scholar] [Publisher Link]

[11] Robert V. Schulte et al., "Database of Lower Limb Kinematics and Electromyography during Gait-Related Activities in Able-Bodied Subjects," *Scientific Data*, vol. 10, no. 1, pp. 1-10, 2023. [CrossRef] [Google Scholar] [Publisher Link]

[12] Junyo Boo et al., "Comprehensive Human Locomotion and Electromyography Dataset: Gait120," *Scientific Data*, vol. 12, no. 1, pp. 1-10, 2025. [CrossRef] [Google Scholar] [Publisher Link]

[13] Jiashuai Wang et al., "Action Recognition of Lower Limbs based on Surface Electromyography Weighted Feature Method," *Sensors*, vol. 21, no. 18, pp. 1-17, 2021. [CrossRef] [Google Scholar] [Publisher Link]

[14] Junyao Wang, Yuehong Dai, and Xiaxi Si, "Analysis and Recognition of Human Lower Limb Motions based on Electromyography (EMG) Signals," *Electronics*, vol. 10, no. 20, pp. 1-21, 2021. [CrossRef] [Google Scholar] [Publisher Link]

[15] Congcong Zhou et al., "Ankle Foot Motion Recognition based on Wireless Wearable sEMG and Acceleration Sensors for Smart AFO," *Sensors and Actuators A: Physical*, vol. 331, 2021. [CrossRef] [Google Scholar] [Publisher Link]

[16] Xingjian Wang et al., "sEMG-based Consecutive Estimation of Human Lower Limb Movement by using Multi-Branch Neural Network," *Biomedical Signal Processing and Control*, vol. 68, 2021. [CrossRef] [Google Scholar] [Publisher Link]

[17] Bruno Dutra, Antonio Silveira, and Antonio Pereira, "Grasping Force Estimation using State-Space Model and Kalman Filter," *Biomedical Signal Processing and Control*, vol. 70, 2021. [CrossRef] [Google Scholar] [Publisher Link]

[18] Kaitlin G. Rabe, Tommaso Lenzi, and Nicholas P. Fey, "Performance of Sonomyographic and Electromyographic Sensing for Continuous Estimation of Joint Torque during Ambulation on Multiple Terrains," *IEEE Transactions on Neural Systems and Rehabilitation Engineering*, vol. 29, pp. 2635-2644, 2021. [CrossRef] [Google Scholar] [Publisher Link]

[19] Christian Morbidoni et al., "Machine-Learning-based Prediction of Gait Events from EMG in Cerebral Palsy Children," *IEEE Transactions on Neural Systems and Rehabilitation Engineering*, vol. 29, pp. 819-830, 2021. [CrossRef] [Google Scholar] [Publisher Link]

[20] Jingxuan Liu, Qing Tao, and Bin Wu, "Dynamic Muscle Fatigue State Recognition based on Deep Learning Fusion Model," *IEEE Access*, vol. 11, pp. 95079-95091, 2023. [CrossRef] [Google Scholar] [Publisher Link]

[21] Stefan Haufe et al., "Gait Event Prediction using Surface Electromyography in Parkinsonian Patients," *Bioengineering*, vol. 10, no. 2, pp. 1-16, 2023. [CrossRef] [Google Scholar] [Publisher Link]

[22] Andrea Tigrini et al., "Phasor-Based Myoelectric Synergy Features: A Fast Hand-Crafted Feature Extraction Scheme for Boosting Performance in Gait Phase Recognition," *Sensors*, vol. 24, no. 17, pp. 1-15, 2024. [CrossRef] [Google Scholar] [Publisher Link]

[23] Alessandro Mengarelli et al., "Myoelectric-based Estimation of Vertical Ground Reaction Force during Unconstrained Walking by a Stacked One-Dimensional Convolutional Long Short-Term Memory Model," *Sensors*, vol. 24, no. 23, pp. 1-19, 2024. [CrossRef] [Google Scholar] [Publisher Link]

[24] Ye Ye et al., "Online Pattern Recognition of Lower Limb Movements based on sEMG Signals and its Application in Real-Time Rehabilitation Training," *Robotica*, vol. 42, no. 2, pp. 389-414, 2024. [CrossRef] [Google Scholar] [Publisher Link]

[25] Shing-Hong Liu et al., "Estimating Gait Parameters from sEMG Signals using Machine Learning Techniques under Different Power Capacity of Muscle," *Scientific Reports*, vol. 15, no. 1, pp. 1-15, 2025. [CrossRef] [Google Scholar] [Publisher Link]